National Radio astronomy Observatory
PO Box O, socorro, NM 87801

VLA TEST Memo. 184

ESTIMATING TROPOSPHERIC PHASE VARIATIONS FOR THE VLA

D. S. Bagri
Feb. 14, 1994

ABSTRACT

It appears that there is a good correlation between the interferometer phase variations due to troposphere and changes in the difference of system temperatures for the two antennas forming the interferometer. This memo describes results of test observations to estimate the tropospheric phase variations using system temperature measurements for the VLA.

INTRODUCTION

Atmospheric water vapor causes increase in the affective pathlength of the radio signals passing thru it. It also causes attenuation of the signals reaching the antenna, which ofcourse also affects the antenna system temperature. Zivanovitch (1993, Thesis, Univ. California, Berkeley) has shown, using BIMA at 3.4 mm, that there is a good correlation between variations of an interferometer phases due to atmospheric water vapor and changes in the difference of the system temperatures for the two antennas forming the interferometer.

Stability of antenna electronics for interferometers, to measure the system temperature variations using total power measurements, is generally not adequate for estimating the tropospheric phase changes. For the VLBA antennas tropospheric phase variations can be estimated using amplitudes of the pulse calibration signals (VLBA Memo No. 691). However in the case of VLA, it is not convinient to use pulsecal system because the fringe rotation is applied in the local oscillator signal at each antenna. Also, unlike VLBA, the VLA does not have electronics required for detecting pulsecal signals coherently. In this memo we describe results of the VLA test observations at 22 GHz using synchroneous detector outputs as indication of system temperature variations, and their use for estimating atmospheric phase variations.

ACCURACY REQUIRMENTS FOR MEASUREMENTS of T_{sys} VARIATIONS

Table 1 shows expected system temperature changes due to tropospheric pathlength variations at several frequencies above 15 GHz. These results are based on atmospheric opacity calculations by Schwab and Hogg (1989, mmA Memo No. 58), and assuming affective tropospheric temperature of 260 °K. Last column in the table gives accuracy needed for estimating the tropospheric pathlength changes to $\lambda/30$. For system temperature values of about 100-150 °K (VLA system temperature values at high frequency bands), this amounts to estimating the system temperature variations accurate to about 1 part in 10^3 at frequencies $\geq$ 20 GHz. Here we have assumed a requirement of $\lambda/30$ measurement accuracy ($\theta_{rms} \approx 1/5$ radian) for the phase variations due to the tropospheric changes. This should give peak to rms sidelobe errors $\approx N/\theta_{rms} \geq 10^2$

(Perley, 1985, NRAO Synthesis Workshop p164) due to rms phase error, θ_{rms}, and (N=) 27 antennas of the VLA telescope.

METHODS OF MEASURING T_{sys} VARIATIONS

(1) Using total power measurements: Total power detector output P=kTBG, where k=Boltzman constant, T=system temperature, B=receiver bandwidth, and G=receiver gain. For reasonable detector input level and receiver parameters, we have to provide atleast about 80 dB of receiver gain before the signal is given to the detector. Power supply and ambient temperature changes amongst other things effect the receiver stability. Our experience with the VLA/VLBA electronics suggests gain variations with ambient temperature giving $(\Delta G/\Delta T) \approx 1dB/300dB/°C$, which suggests that it will be difficult to achieve gain stability of 10^3 even if the receiver temperature is controlled to 0.1° C. In addition, other changes like power supply voltage variations etc. are going to effect the total power measurements.
(2) Alternate methods: Amplitude measurements of the pulse calibration signal injected at the receiver input, as used in VLBI, can be used to estimate the system temperature (VLBA Electronics Memo No. 137). This approach is possible for the VLBA, but cannot be easilly used in the VLA due to the fringe rotation applied in the local oscillator signal at the antennas. Also coherent detection of the pulsecal tones requires specilized hardware which is not available on the VLA.

In the VLA a known amount of broadband noise calibration signal is injected at the input of each receiver on every antenna. The noise signal is modulated on/off at half the waveguide cycle rate. The system temperature is estimated using measurements of the total power (fixed to 3.0 Volts by ALC in the antenna frontend electronics) and the synchroneous detector outputs. From radiometric equation $(\Delta T_{sys}/T_{sys} = 2(T_{sys}/T_{cal})/\sqrt{B\tau})$, for the overall VLA bandwidth of 200 MHz, an integration period of two seconds, and for the noise calibration signal = 10% of the system temperature we should be able to measure T_{sys} variations with better than 10^{-3} accuracy. (The monitor system quantization errors may limit it at somewhat lower value). The stability of typical diode noise sources is about 0.1% for 1°C and 0.25% power supply variations. The detector circuit stability as measured for the VLBA system is better than $10^{-3}/°C$. If other systematics are not limiting, the system temperature changes should be useful for estimating the atmospheric phase variations with accuracy of about $\lambda/30$.

TEST OBSERVATIONS AND RESULTS

Calibration radio source 3C286 was observed with the VLA using the k-band default settings for the continuum observations (22.46 GHz) on 93OCT05 when the array was in DnC (north arm in C and east and west arms in D) configuration. AIPS was used for extracting the (pseudo) system temperature data (using TY table) for all four IFs, and then these were combined to give system temperature values every alternate 10 seconds. Also antenna phases were calculated every 20 seconds using CALIB. A total of about 40 minutes of data were obtained. In figure 1 trace 1 shows phase between antenna 13 (located at N18) and antenna 1 (located at N16), and trace 2 shows difference of system temperature for the two antennas. From the two plots it appears that there is a good correlation between the phase changes and difference between the system temperature for the two antennas. However we donot have an accurate knowledge of relative scales of

system temperatures for these antennas, and therefore taking a simple difference can give erroneous results for the system temperature differences. Also we donot have a good knowledge of relationship between the atmospheric phase variations and resulting system temperature changes. This may be dependent on the atmospheric temperature profile and pressure etc.

Fortunately we can do a simple least square fitting between the phase variations and the temperature changes on calibration sources to find the proportionality constant for each antenna (telling how the antenna phase is effected using the system temperature changes). We can then use these coefficients alongwith the system temperature variations for predicting the atmospheric phase corrections while observing target sources.

We used first 20 minutes of data for determining the proportionality constants by using LSF in expression

$$\Phi_{mni} - (\alpha_{mi}T_{mi} + \alpha_{ni}T_{ni} + \beta_{mn})$$

where Φ_{mni} is the phase between antennas m and n, i is time series, α_m, and α_n are proportionality constants for antennas m and n, T_m and T_n are system temperature measurements for antennas m and n, and β_{mn} is constant offset term for the baseline. We analysed the data for different antennas forming baselines with antenna 20 (located on E1) as the reference antenna. The values of the coefficients are given in Table 2. Also the table gives location of these antennas and the pre fit rms phase for each baseline. We used these values of coefficients to estimate expected atmospheric phase variations using the system temperature changes for the (1) first 20 minutes of data, (2) entire 40 minutes of data, and (3) second 20 minutes of data. The RMS of the difference between the measured and expected values for the phases for (1) the first 20 minutes (fit range), (2) entire 40 minutes interval (full range), and (3) second 20 minute duration (outside the fit range) are given in the table. It seems the phase stability of the antennas beyond E4 on the east arm was affected much more than antennas with comparable baseline lenths on other two arm, and is probably due to instrumental reasons. Therefore we will not consider phase stability of these antennas here. From the results it is seen that there is improvement from prefit rms phase of about 40° to outside fit range rms phase of about $20 - 25°$ for baselines $\leq 0.7km$, and similarly from about 80° to about 45° for baselines upto 1.7 km. However the coefficient for the reference antenna is varying vastly from baseline to baseline. Also the values of rms phases for the fit range, full range and outside the fit range vary quite a bit.

Next, we removed constant phase offset and took average values of the coefficients (calculated over several baselines) for each of the antennas 1, 13, and 20, and recalculated the predicted interferometer phases for the baselines formed by these antennas. The resulting rms of the difference (between predicted and observed) phases for the fit range, full range and outside the fit range for baselines formed by antennas 1 and 20, and antennas 13 and 20 are as shown in Table 3. The rms phases for each of the baseline seems similar for all the three fitting durations, and also give lower rms phase for the duration outside the fit range. This suggests that the average values of the coefficients are more representative of the reality than the values calculated for each baseline indepedently. Therefore we should explore using "global" fitting to determine the coefficients of proportionality between the system temperature measurements and the tropospheric phase variations.

CONCLUSION

During the test observations with the VLA antennas at 22 GHz we observed a good correlation between phase variations of the interferometers due to troposphere and the difference of the system temperature for the antennas forming the interferometers. For baselines $\lesssim 0.7$ km the rms phase reduced from about 40 ° to $\lesssim 25°$, and for the baselines between 0.7 to about 1.8 km the rms phases ranging from 50° to 80° improved by almost a factor of 2. Further it appears that we need to explore the possibility of using "global" fitting for determining the proportionality constants between the tropospheric phases and the system temperature measurements. The corrected interferometer phases seem to have much larger variations than expected from the receiver thermal noise. Therefore to understand limitations/usefulness of this method we need to understand if there are sources other than troposphere causing the phase changes and the system temperature variations and their extent.

FIGURE 1 — Interferometer phase variations (trace 1) and difference of system temperatures (trace 2) while observing calibration source 3C286 at 22.46 GHz. (Baseline length = .33 km)

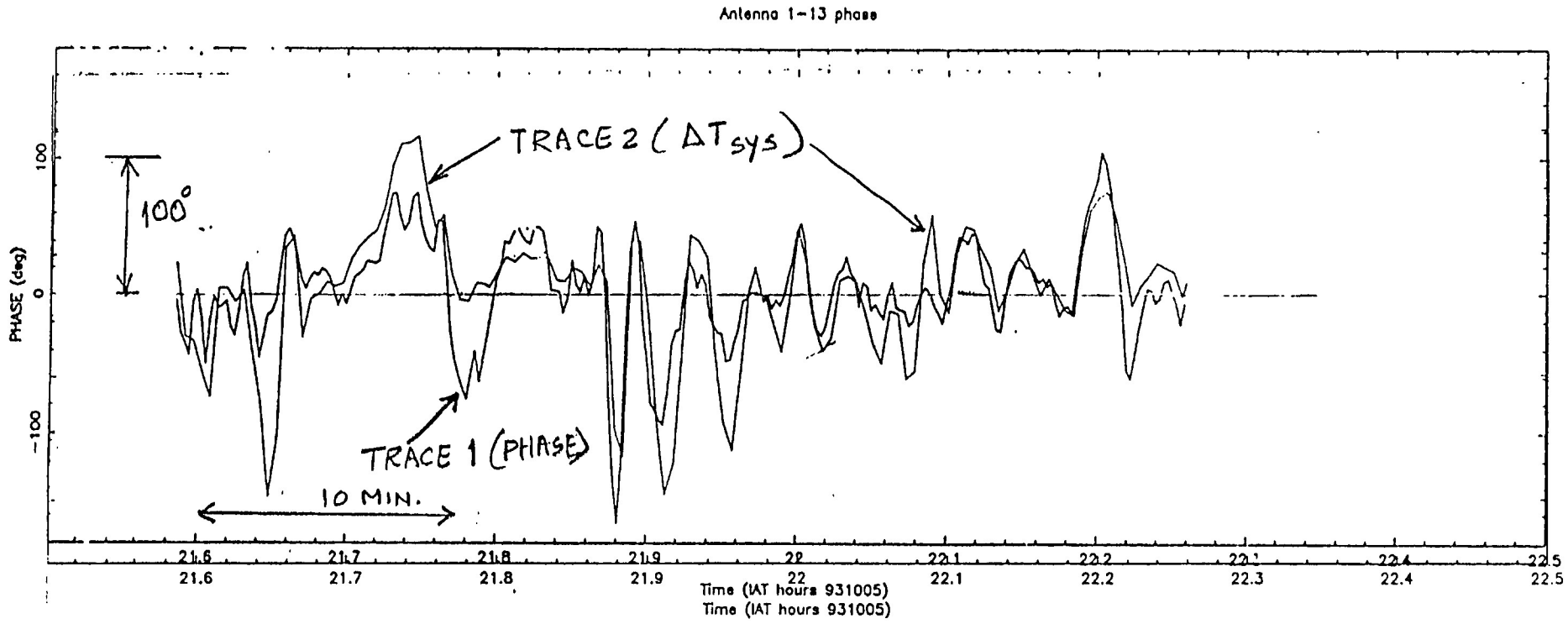

FREQ (GHz)	ATMOSPHERIC * ATTENUATION (Np) FOR PWV OF .5 mm	4 mm	8 mm	ΔT_{ATM} °K/mm	°K/λ	°K/$\frac{\lambda}{30}$ **
20	7.7×10^{-3}	21.1×10^{-3}	32.1×10^{-3}	.24	3.6	.12
22	1.26×10^{-2}	4.18×10^{-2}	7×10^{-2}	.6	7.8	
45	6.1×10^{-2}	9.8×10^{-2}	10.7×10^{-2}	.5	3.5	.12
86	$.765\times10^{-2}$	4×10^{-2}	6.86×10^{-2}	.6	2.4	.08
115	.1556	.275	.327	1.3	3.6	.12
230	.03	.2225	.45	4	5.2	.18
350	.1	.803	1.733	16	12	.4

* DATA FROM SCHWAB (MMA Memo. 58)

** λ/30 TO GIVE DYNAMIC RANGE = $\frac{N}{\theta_{RMS}}$ ~200 for MMA

TABLE 1 — Expected system temperature changes due to atmospheric water vapor at different frequencies.

TABLE 2 — Results of Test observations at 22.4 GHz on 3C286 for estimating atmospheric phase corrections using T_{sys} variations.

ANT. # Ref. ANT 20 ON E1	LOC	DIST FROM REF. ANT (km)	Pre fit RMS ϕ (ϕ_{rms}) (deg)	POST FIT RMS PHASE			FIT COEFFS.	
				FIT RANGE (σ)	FULL RANGE (σ_f)	OUT OF FIT RANGE (σ_o)	a_1 $\times 10^3$	a_2 $\times 10^3$
23	E2	.05	11.3	7.7	11.2	14.0	-1.57	1.924
16	E3	.085	12.7	8.8	10.9	13.1	-1.648	2.359
4	E4	.14	26.5	13.3	28.6	38.7	-1.948	1.948
7	E5	.21	25.9	16.0	26.7	34.7	-1.443	2.209
18	E6	.29	31.7	17.2	28.8	37.4	-1.842	2.556
24	E7	.385	37.4	17.1	29.8	38.8	-1.761	2.563
5	E8	.48	51.9	37.6	54.6	69.9	-1.375	2.203
17	E9	.59	59.4	18.9	45.0	62.2	-2.078	2.703
3	W2	.05	13.1	9.7	10.9	12.2	-1.869	1.92
28	W3	.09	15.7	13.2	14.2	15.6	-1.912	2.066
2	W4	.15	20.0	14.7	14.6	15.1	-1.52	2.157
21	W5	.22	21.1	16.3	15.2	14.9	-2.089	1.932
10	W6	.30	22.9	19.1	18.2	17.8	-1.325	1.501
8	W7	.39	27.4	22.9	20.9	19.3	-1.432	1.318
9	W8	.49	30.0	22.9	23.9	25.6	-1.227	1.61
14	W9	.60	35.5	23.9	24.4	26.2	-2.162	1.196
22	W10	.71	41.3	22.6	26.4	30.5	-2.447	1.906
25	N2	.06	20.3	13.9	17.1	20.1	-1.695	2.003
19	N4	.135	24	17.2	19.8	22.5	-1.491	1.81
6	N6	.27	30.2	17.9	20	22.4	-1.925	2.215
27	N8	.44	35.2	20.1	21.7	23.8	-1.596	2.025
11	N10	.65	43.4	24.1	26.3	29	-1.907	2.009
26	N12	.89	54.8	22.1	30.1	36.7	-2.622	2.041
15	N14	1.15	66.4	30.9	34.9	39.4	-2.074	1.196
1	N16	1.44	75.3	33.1	37.1	42.5	-2.749	2.291
13	N18	1.76	80.1	28.5	36.9	43.8	-3.172	2.269

ANT. # Ref. ANT 20 ON E1	LOC	DIST FROM REF. ANT (km)	Pre fit RMS ϕ (ϕ_{rms}) (deg)	POST FIT RMS PHASE		
				FIT RANGE (σ)	FULL RANGE (σ_f)	OUT OF FIT RANGE (σ_o)
1	N16	1·44	75·3	37·6	36·4	36·9
13	N18	1·76	80·1	36·7	36·7	36·8

Table 3 — Results for two baselines when average values of coefficients are used for estimating atmospheric phase changes